Analysis of sub-visible particles in complex injectable formulations

Sediq, A.S.

Chapter 3

Protein-polyelectrolyte interactions: monitoring particle formation and growth by nanoparticle tracking analysis and flow imaging microscopy

Ahmad S. Sediq[1], M. Reza Nejadnik[1], Inas El Bialy[1], Geert J. Witkamp[2], and Wim Jiskoot[*,1]

[1] Division of Drug Delivery Technology, Leiden Academic Centre for Drug Research (LACDR), Leiden University, 2333 CC Leiden, The Netherlands

[2] Biotechnology Department, Delft University of Technology, 2628 CA Delft, The Netherlands

The chapter was published in the *European Journal of Pharmaceutics and Biopharmaceutics: Eur J Pharm Biopharm 2015 93: 339-345*

Abstract

The purpose of this study was to investigate the formation and growth kinetics of complexes between proteins and oppositely charged polyelectrolytes. Equal volumes of IgG and dextran sulfate (DS) solutions, 0.01 mg/ml each in 10 mM phosphate, pH 6.2, were mixed. At different time points, samples were taken and analyzed by nanoparticle tracking analysis (NTA), Micro-Flow Imaging (MFI) and size-exclusion chromatography (SEC). SEC showed a huge drop in monomer content (approximately 85%) already 2 minutes after mixing, while a very high nanoparticle (size up to 500 nm) concentration (ca. $9x10^8$/mL) was detected by NTA. The nanoparticle concentration gradually decreased over time, while the average particle size increased. After a lag time of about 1.5 h, a steady increase in microparticles was measured by MFI. The microparticle concentration kept increasing up to about $1.5x10^6$/mL until it started to slightly decrease after 10 h. The average size of the microparticles remained in the low-µm range (1-2 µm) with a slight increase and broadening of the size distribution in time. The experimental data could be fitted with Smoluchowski's perikinetic coagulation model, which was validated by studying particle growth kinetics in IgG:DS mixtures of different concentrations. In conclusion, the combination of NTA and MFI provided novel insight into the kinetics and mechanism of protein-polyelectrolyte complex formation.

Introduction

The interaction between proteins and polyelectrolytes has been receiving increasing attention in pharmaceutical sciences because of the growing importance of protein drugs[1]. The latter is mainly related to their specificity and the lack of toxic metabolites, resulting in considerably less interference with untargeted biological processes and, hence, less adverse effects and increased clinical efficiency[2]. Successfully developing protein drugs, however, requires the availability of highly pure protein batches as well as suitable formulations that guarantee the physical and chemical stability of the protein[3-5] until its delivery at the target site.

Polyelectrolytes are a major group of the macromolecules that have shown to offer advantages in purification[6,7], stabilization[8] and delivery of therapeutic proteins[9,10]. Polyelectrolytes are suitable as component of protein delivery systems because they can be selected with specific hydrophilicity, versatile charge properties, biodegradability, natural origin, and roles in preventing aggregation and denaturation of proteins[11-14]. Moreover, polyelectrolytes have been used to increase the amount of protein loaded onto the surface of solid microneedles and microparticles via layer-by-layer deposition of oppositely charged proteins and polyelectrolytes[15,16]. Furthermore, polyelectrolyte-mediated precipitation methods have been used in protein purification processes[17] to decrease the number of isolation steps at a low cost. This approach is considered to be more selective than the use of other precipitants, such as ammonium sulfate or organic solvents[18]. In addition, another advantage of polyelectrolyte-assisted precipitation along with protein co-precipitation techniques[19] is that these methods do not require organic solvents that could be harmful to the protein as well as the environment. The molecular interaction involves electrostatic interactions between charged surfaces of the protein and oppositely charged groups of the polyelectrolyte[20]. The onset of complexation depends on several parameters, such as pH, ionic strength, protein/polyelectrolyte ratio and physico-chemical characteristics of the protein and the polyelectrolyte (e.g., charge, size)[21,22]. These interactions create insoluble complexes, which then aggregate further to form larger particles that will eventually precipitate from the solution[23]. The process of particle growth depends not only on the nature of the particles, but also on external factors, such as temperature, stirring and sedimentation[24].

A great challenge in the direct assessment of protein-polyelectrolyte interactions has been the lack of techniques that are able to simultaneously detect, characterize and quantify (sub)visible particles that form upon complexation of protein and polyelectrolyte. Emerging particle analysis techniques[25,26], however, may provide reliable ways to monitor protein-polyelectrolyte complex formation and growth. In the nanometer range, nanoparticle tracking analysis (NTA) is a valuable technique that counts and sizes particles in a suspension. In

the flow-cell of NTA, the particles scatter a beam of laser light, which is detected through a microscope and recorded into a video exhibiting the movement of particles in the suspension. The displacement of individual particles, or the Brownian motion, in a plane is tracked in time to deduce the individual particle size[27-30]. In the micrometer size range, flow imaging microscopy techniques, such as, Micro-Flow Imaging (MFI), are currently gaining ground as established methods for micron-size particle sizing and counting[31-34]. The principle of detection is based on the change in the light intensity passing through a particle compared to the background. Based on the captured images the particle size and count are derived. The same images can be used to assess several morphological aspects of individual particles, like aspect ratio and transparency. The aim of this study was to develop a method based on the combination of NTA and MFI to monitor and characterize the process of particle formation and growth during protein-polyelectrolyte complexation, assisted by size-exclusion chromatography (SEC) to quantify the amount of unbound protein monomer. A monoclonal antibody was used as a model protein and dextran sulfate as a model polyelectrolyte. The experimental data for a few different experimental conditions were fitted with Smoluchowski's perikinetic coagulation model[35,36].

Materials and Methods

Materials

Dextran sulfate (from Leuconostoc spp., Mw = 5000), sodium phosphate dibasic dihydrate, sodium phosphate monobasic dihydrate, sodium azide and sodium sulfate (pKa < 2) were obtained from Sigma (Sigma-Aldrich, Steinheim, Germany). Ultrapure water (18.2 MΩ.cm) was dispensed by using a Purelab Ultra water purification system (ELGA LabWater, Marlow, UK). A monoclonal human IgG1 subclass (IgG; pI = 8.4), formulated at 65 mg/ml in 10 mM sodium citrate buffer containing 5% sucrose at pH 6.0, described before[29,37,38], was used as a model protein. Stock solutions of 0.01 mg/ml of IgG in aqueous solution of 10 mM phosphate buffer, pH 6.2 (filtered by using a 0.22-µm polyethersulfone-based syringe driven filter unit (Millex GP, Millipore, Ireland)), was prepared. The same buffer was used to prepare stock solutions of 0.01 mg/ml dextran sulfate. In preliminary studies we found that a low buffer concentration and a pH value lower than 7 are beneficial for the formation of IgG-dextran sulfate complexes. Addition of the protein or polyelectrolyte had no effect on the pH of 6.2.

Mixing, incubation and sampling procedure

A volume of 13 mL of the IgG stock solution was poured into a graduated glass cylinder (Duran®, Hirschmann, Eberstadt, Germany), with an inner diameter of 1.4 cm and a height of 14.9 cm. 13 mL of the dextran sulfate stock solution was added to the IgG solution.

Subsequently, the IgG/dextran sulfate mixture was homogenized by gentle pipetting up and down 15 times, and then incubated for a period of 14 hours. In order to avoid unwanted movements and temperature fluctuations (as these might affect the kinetics of the particle growth), the glass container was kept on a sturdy bench where the analytical instruments were located. The first sample was taken immediately after mixing. The sampling was continued for 840 min after preparation according to the scheme shown in Figure 1.

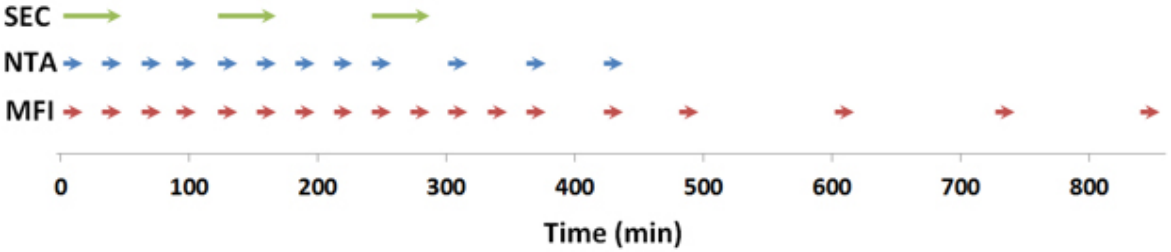

Figure 1: Schematic overview of the sampling time points for each type of measurement performed in this study. The length of each rod indicates the approximate analysis time per sample, including sample pretreatment and handling.

Samples were directly used for the different analyses, unless otherwise stated. The experiment was performed twice. During the experiment the room temperature in the lab was monitored (23 ± 0.8 °C). In order to prepare samples for quantification of the free protein monomer content, 1 mL of the sample was centrifuged in a 1.5 mL Eppendorf tube at 18,000 ×g for 15 minutes. A hundred µL from the top part of the liquid was taken and immediately used for measurement of the monomer content by using SEC. The supernatant was analyzed by NTA to confirm that it was free of particles (results not shown).
In order to check the applicability of the method to other formulations and to validate whether Smoluchowski's perikinetic coagulation model (see below) describes the particle formation process, additional mixing experiments were performed with two different concentrations of IgG and dextran sulfate in the starting materials, namely 0.005 and 0.02 mg/mL (instead of 0.01 mg/mL). The experimental procedure was kept the same, except that the particle formation process was monitored for only 270 min.

Size-exclusion chromatography

High pressure size-exclusion chromatography (SEC) was performed to quantify the amount of free IgG monomer in the solution in absence and presence of dextran sulfate. This was executed on an Agilent 1200 chromatography system (Agilent Technologies, Palo Alto, California) combined with a Wyatt Eclipse (Wyatt Technology Europe GmbH, Dernbach, Germany). A Yarra 3 µm SEC-2000 column (300 × 7.8 mm) coupled with a Yarra Security Guard precolumn (Phenomenex, Torrance, CA, USA) was used. Centrifuged

(18,000 x g for 15 minutes) samples (100 µL) were injected and separation was performed at a flow rate of 0.5 mL/min. The mobile phase consisted of 100 mM sodium phosphate, 100 mM sodium sulfate, and 0.05 % w/v sodium azide at pH 7.2. Ultraviolet absorption detection was performed at 280 nm. In order to calculate the monomer decrease after complexation, the areas under the curve (AUC) of the UV signal were used.

Nanoparticle tracking analysis

NTA was performed at room temperature (23 ± 0.5°C) with a NanoSight LM20 (NanoSight Ltd., Amesbury, United Kingdom) equipped with a 640 nm laser and operating at an angle of 173° with respect to the flow cell (100 x 80 x 10 µm). Samples were taken from the mixture vessel by using a sterile 1 mL syringe (BD Discardit II, New Jersey). The contents of the syringe were injected into the chamber by an automatic pump (Harvard apparatus, Catalog no 98-4362). For each sample a 90 s video was captured with shutter set at 1495 and gain at 400. The video was analyzed by using the NTA 2.0 Build 127 software. The following settings were used for tracking of the particles: background extract on; brightness 0; gain 1.00; blur size 3x3; detection threshold 10, viscosity equal to that of water. All other parameters were set to the automatic adjustment mode.

Flow imaging microscopy

A Micro-Flow Imaging (MFI) system (MFI5200, ProteinSimple, Santa Clara, USA), equipped with a silane coated flow cell (1.41 x 1.76 x 0.1 mm) and controlled by the MFI View System Software (MVSS) version 2, was used for flow imaging microscopy analysis. The system was flushed with 4 mL purified water at 6 mL/min prior to each measurement. The flow cell cleanliness was checked visually between measurements. The background was zeroed by flowing 10 mM phosphate buffer, pH 6.2, and performing the 'optimize illumination' procedure. Samples of 0.5 mL with a pre-run volume of 0.2 mL were analyzed at a flow rate of 0.17 mL/min and a fixed camera rate of 22 flashes per second.

The data recorded by the MVSS was analyzed with MFI View Analysis Suite (MVAS) version 1.2. For each sample, stuck, edge and slow moving particles were removed by the software before data analysis. The equivalent circular diameter (ECD), which is the diameter of a circle that has an area equal to that of the particle imaged by MFI, was calculated and presented as a measure of the particle size.

Theoretical calculations

Fitting the experimental data with Smoluchowski's perikinetic coagulation model

The experimental data were plotted such that they illustrate the changes in total particle concentration over time, as particle collision leads to fusion into larger particles. These

changes were fitted by a one-phase exponential decay equation:

$$N(t) = N_0 e^{-\frac{ln2}{\tau_{exp}}t} \quad \textbf{Eq. 1}$$

from which N_0 (the initial total particle concentration) and τ_{exp} (the experimental half-life, i.e., the time at which the total concentration of particles reduces to half) were obtained. Knowing the initial total number of particles N_0, Smoluchowski's perikinetic coagulation theory was used to predict a theoretical half-life (τ_{theor}) by assuming that all particle collisions lead to fusion:

$$\tau_{theor} = \frac{3\mu}{4K_B T {N_0}^2} \quad \textbf{Eq. 2}$$

where μ is the viscosity of the buffer, K_B the Boltzmann constant and T the absolute temperature. The sticking probability (α), defined as the fraction of particles remaining in contact after collision[24], was calculated from the ratio between τ_{theor} and τ_{exp}:

$$\alpha = \frac{\tau_{theor}}{\tau_{exp}} = \frac{3\mu}{\tau_{exp} 4\mathrm{K_B T} {N_0}^2} \quad \textbf{Eq. 3}$$

Equation 1 was used to fit the experimental data for measurements with different starting concentrations (using GraphPad Prism version 5). Subsequently, the collision efficiency for each condition was calculated and compared.

Results

In order to monitor the particle formation and growth we performed simultaneous NTA and MFI measurements at different time points after mixing equal volumes of IgG and dextran sulfate solutions, yielding a final concentration of 0.05 mg/ml IgG and 0.05 mg/ml dextran sulfate. The amount of free IgG was measured by SEC after spinning down the formed particles.

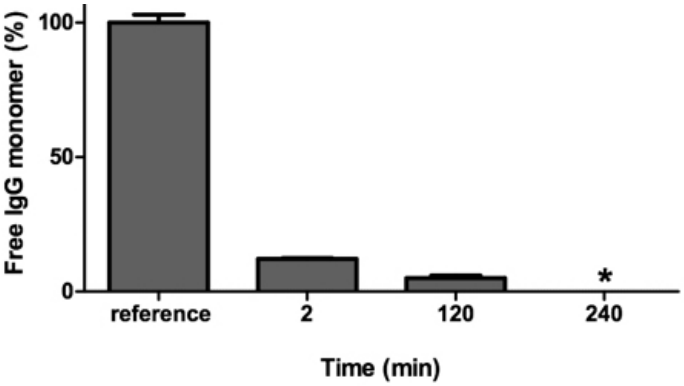

Figure 2: SEC results of centrifuged IgG/dextran sulfate (1:1 w/w, total concentration 0.01 mg/ml) mixtures, shown as percentage of IgG left in the solution at different incubation time points. The reference bar is 0.01 mg/ml IgG solution diluted twofold with 10 mM phosphate buffer, pH 6.2. The measurement at 4 hours after preparation did not show any IgG peak at all (*).

The amount of free IgG monomer in the control (IgG alone) and prepared dextran sulfate/IgG mixture taken at three specified time points (see Figure 1) as measured by SEC is shown in Figure 2. The appearance of the pellet after spinning down the mixture was a solid precipitate.

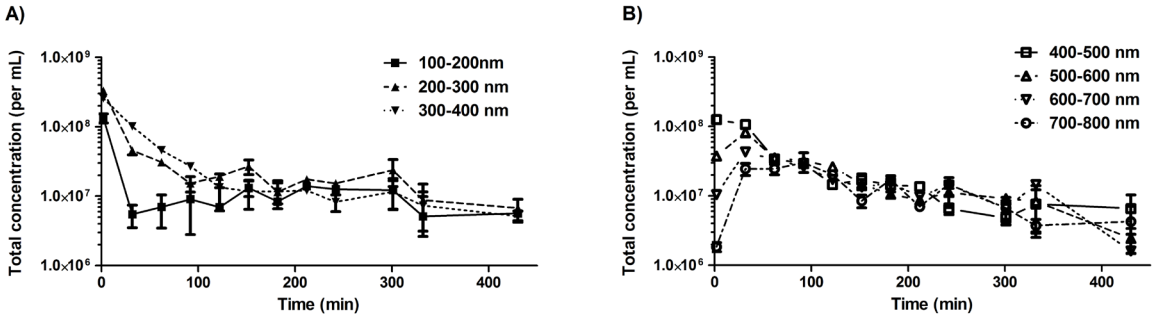

Figure 3: Results of NTA of IgG/dextran sulfate (1:1 w/w, total concentration 0.01 mg/ml) mixtures as function of incubation time. Graphs show the total particle concentrations (logarithmic scale) for each 100-nm wide size category within the size range between 100-800 nm at different time points (A: 101-400 nm; B: 401-800 nm). The size categories were split into two graphs for sake of clarity. The results of duplicate experiments are incorporated in the graphs, where each dot represents the mean and the bars the highest and lowest value. The connecting lines serve as a guidance to clarify the progress of the particle concentration of the different populations.

Compared to the reference sample, all samples showed a great decrease in free IgG monomer content, down to 12%, 5% and 0%, at 2, 120 and 240 min, respectively, after starting the incubation. Even though this SEC column showed to be suitable to separate

up to IgG tetramers, no oligomer peaks were detected by SEC for any of the samples, suggesting that the IgG monomers are rapidly included in particles that are too large to pass the SEC column and/or particles that are spun down during the centrifugation step prior to SEC analysis.

Nanoparticle tracking analysis (NTA)

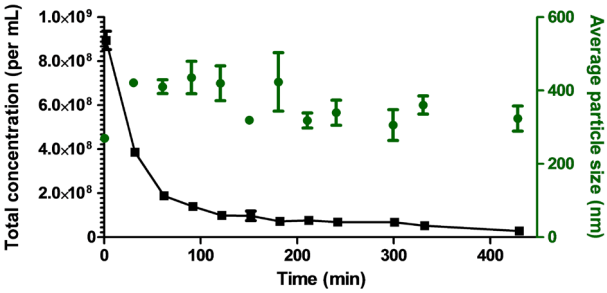

Figure 4: Total particle concentration within the 100-800 nm size range (black squares) and average particle size (green circles) of IgG/dextran sulfate (1:1 w/w, total concentration 0.01 mg/ml) mixtures, measured with NTA as function of experiments are incorporated in the graph, where each data point represents the mean and the bars the higher and the lower value.

The generated size distribution curves obtained from NTA were sliced in segments of 100 nm bins and the total concentrations of particles within these segments at different time points were plotted. The lower detection limit of NanoSight is about 40 nm (depending on the light scattering properties of the particles), therefore the segmentation was started from 100 nm. Size bins over 800 nm were not included because no reliable data could be obtained (further explained in the Discussion section). The total concentrations of particles in the categories between 100 and 500 nm were relatively high and decreased with time already from the beginning (Figure 3A), whereas the larger size ranges showed an increase in particle concentration after the start of the experiment, which gradually stabilized and started to decrease at later time points (Figure 3B). The total nanoparticle concentration (population with a size between 100-800 nm) and the associated average particle size of this population over time are shown in Figure 4. The total particle concentration decreased exponentially with an increase in mean size in the first hour of the study timespan.

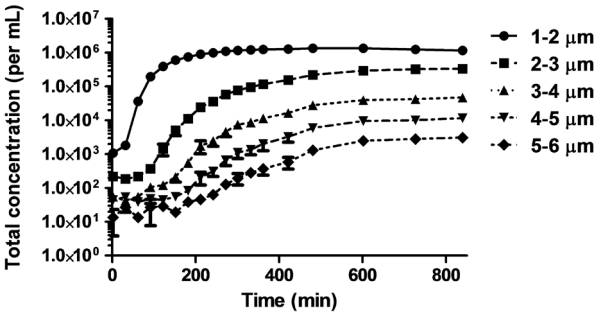

Figure 5: Results of MFI of IgG/dextran sulfate (1:1 w/w, total concentration 0.01 mg/ml) mixtures as function of incubation time. Graph shows the total particle concentrations (logarithmic scale) for each 1-µm wide size category within the size range between 1-6 µm at different time points. The results of duplicate experiments are incorporated in the graph, where each dot represents the mean and the bars the highest and lowest value.

Flow imaging microscopy was used to monitor the concentration and size distribution of particles in the micrometer-size range. Figure 5 shows the particle concentration as function of time, plotted by grouping the particles in 1-µm wide size bins, displayed up to 6 µm (the contribution of larger particles to the total particle count was negligible).

The particle concentration in the size range covered by the MFI instrument started to increase rapidly from about 1.5 hour after the start of the experiment. These particles were mainly in the size range between 1-2 µm. Interestingly, when the rate of increase in the concentration of 1-2 µm particles started to decrease, particles in the range of 2-3 µm began to form at a fast rate; when the increase in concentration of the latter size range started to level off, 3-4 µm sized particles started to form. Similar trends continued to happen successively for the larger particle sizes too. The total concentration of µm-range particles increased over time and reached its maximum at about 10 h, after which it started to drop gradually, while the average size of the particles increased gradually over time after an apparent decrease within the first minutes of the experiment (Figure 6).

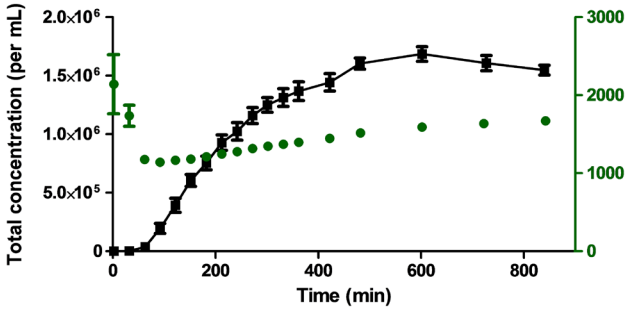

Figure 6: Total particle concentration within the 1-6 µm size range (black squares) and average particle size (green circles) of IgG/dextran sulfate (1:1 w/w, total concentration 0.01 mg/ml) mixtures, measured with MFI as function of incubation time. The results of duplicate experiments are incorporated in the graph, where each data point represents the mean and the bars the higher and the lower value.

NTA and flow imaging microscopy results combined

In order to visualize the overall development of particle formation and growth, as studied

by NTA and MFI, the raw data generated by each method was used to plot the distribution of particles of different sizes over time in a single graph (Figure 7).

This graph shows that a large number of nm-range particles were detected soon after the mixing of the protein and the polyelectrolyte, while no µm-range particles were detected at early time points. The particle size progressively increased with incubation time and the trend was clear toward the formation of µm-range particles within hours and a simultaneous decrease in the number of nm-range particles.

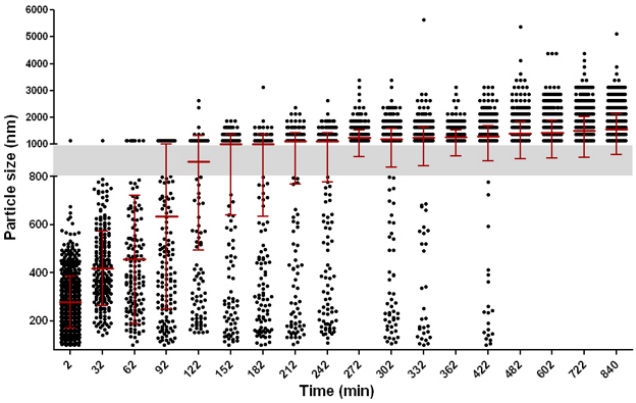

Figure 7: Graphical representation of the particle growth in IgG/dextran sulfate (1:1 w/w, total concentration 0.01 mg/ml) mixtures, as monitored by NTA and MFI (based on the data sets shown in Figures 3-6). Scatter plot shows the size of individual particles (dots) detected by NTA and MFI in a volume of 50 µL at each time point (non-linear time axis). Particles detected by NTA measurements are shown in the lower part (100-800 nm), the ones from MFI in the upper part (1000-6000 nm). The grey bar represents the area that is not covered by both techniques. For each time point, the calculated average size and the corresponding standard deviation are indicated in red.

Fitting the experimental data into Smoluchowski's perikinetic coagulation model

The decrease in total particle concentration measured with NTA and MFI were fitted in a one-phase exponential decay formula (Eq. 1). For the concentration of 0.01 mg/ml the fitted exponential decay resulted in a N_0 value of 1.29×10^9 particles per mL and a τ_{exp} of 12.8 minutes (95% confidence intervals (CI): 8.1 – 31.1 minutes). With the help of Eq. 2 deduced N_0 value, the τ_{theor} was calculated to be 2.5 minutes. The sticking probability can be either calculated by taking the ratio of τ_{theor} to τ_{exp} or directly from the deduced N_0 and τ_{exp} values and the help of Eq. 3. For the condition with 0.01 mg/ml of total material concentration resulted in an average sticking probability of 0.19 (95% CI: 0.08 – 0.31).

The same data fitting approach was applied for two other concentrations with equal IgG:dextran sulfate ratio. The rationale behind the chosen condition was the assumption that the nature of the particles, hence the kinetics of the coagulation, will stay the same. The best-fit curves for the different studied conditions are shown in Figure 8. The curves indicate that the lowest concentration of the mixture shows a much slower decay, hence a larger τ_{exp} (41.6 minutes (95% CI: 25.8 – 107.9 minutes) for a total concentration of

0.005 mg/ml, versus 14.1 minutes (95% CI: 10.2 – 22.6 minutes) for 0.02 mg/ml), compared to the higher concentrations. Note that the NTA measurement of the 0.02 mg/ml sample at the first time point indicated a higher average size, compared to the other concentrations. This indicates that the particle coagulation for that concentration had proceeded to a further stage. Figure 8 also presents the average sticking probabilities (average values: 0.16 for 0.005 mg/ml; 0.19 for 0.01 mg/ml; 0.18 for 0.02 mg/ml). The average values were not significantly different (one-way Anova test: P = 0.9573).

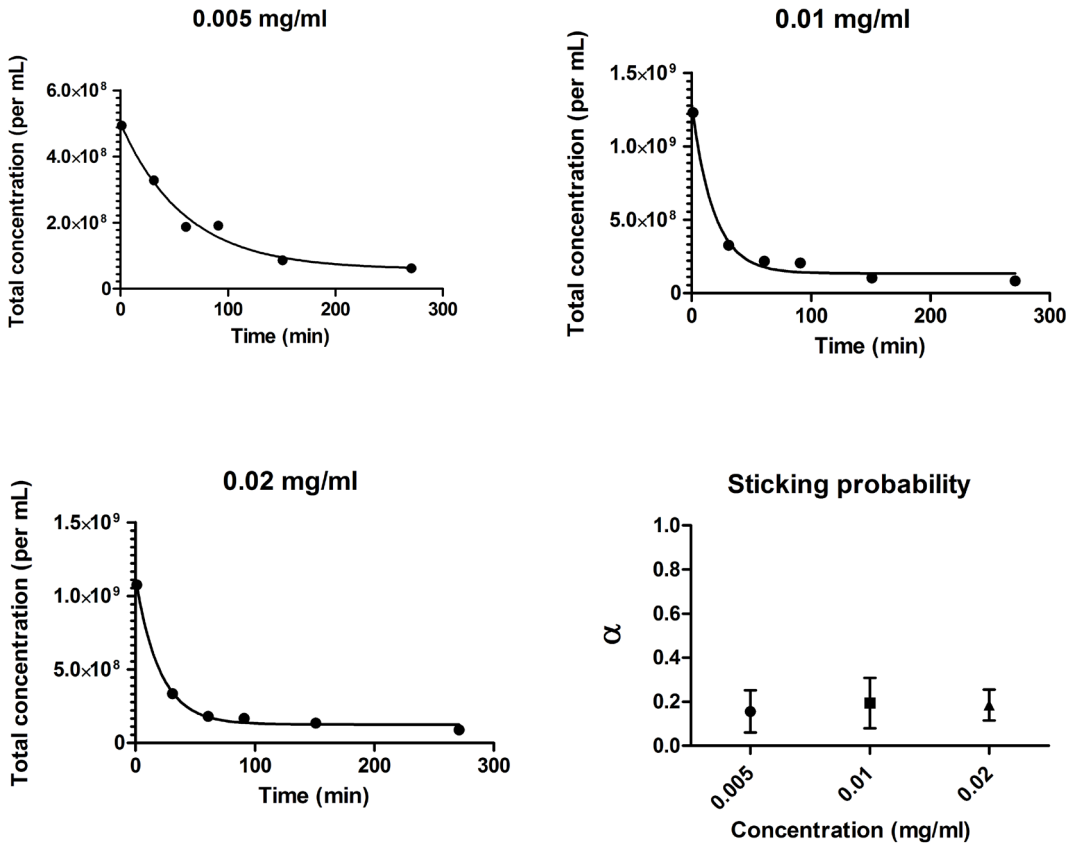

Figure 8: Total particle concentration over time for samples with 0.005, 0.01 and 0.02 mg/ml of each starting solution are shown. The solid lines show the best fit curve gained by using Equation 1 as a model. The graph in lower right corner presents the sticking probability calculated with the help of Equation 2 and 3. The error bars represent the 95% confidence interval.

Discussion

In this study we have shown the applicability of the combination of NTA and MFI for monitoring the particle formation and growth, when a dextran sulfate solution is added to an IgG solution. Analysis of particle concentration and size in both the nanometer- and the

micrometer-size range as function of time provides a good insight into the kinetics of the particle formation process, in terms of both particle size and particle concentration. As soon as the protein and the polyelectrolyte are mixed, the solution becomes supersaturated and electrostatic interactions lead to rapid formation of protein-polyelectrolyte complexes[11]. At this point nucleation occurs with the appearance of primary particles, which is associated with a rapid loss of free monomeric IgG as demonstrated in our study by SEC analysis (Figure 2). This observation is in line with the literature reporting that the stage of aggregation of primary particles[39] into flocks is the rate-limiting step in the formation and growth of larger particles[40].

In this study NTA proved to be a valuable tool to study the interaction kinetics in the early stage, where no micron-sized agglomerates are formed yet. However, the progressive increase in larger particle concentrations made the NTA measurements increasingly difficult to perform and eventually impossible. This is due to inaccuracies caused by the presence of large particles (over 800 nm) with multiple scattering centers that rapidly change position, which erroneously leads to the detection of apparent very small particles
(smaller than 100 nm).

Moreover, their brightness and size leads to masking and overlapping of particles. In addition, above this size the Brownian motion becomes very low, leading to additional inaccuracies[28]. This was the reason for applying NTA only for the first part of the coagulation process (up to 440 min) and excluding the particles with sizes larger than 800 nm and smaller than 100 nm. Continuously decreasing concentrations of particles in the lower nanometer size range (101-400 nm) were accompanied by an initial increase followed by a moderate decrease in concentrations of larger nanoparticles (> 400 nm), as shown in Figure 3. The exponential decrease in total nanoparticle concentration (Figure 4) indicates that over time the smaller particles coagulated in order to form larger particles. However, the average particle size measured by NTA only increased at the start and afterwards remained fairly constant. That can be explained by the chosen lower limit for the NTA data (101 nm), leading to underestimation of the number of smaller particles[29].

In the later stage of the coagulation process, when the particle size entered the micrometer range, MFI took over the role of NTA to monitor particle growth. By displaying the measured microparticle size classes in 1-µm bins, the consistency and precision of the technique in monitoring the particle growth process was revealed (Figure 5). The course of the total particle concentration showed a rapid growth, starting at about 90 minutes, and began to decrease slightly after about 600 minutes (Figure 6). This indicates that around this moment the low-nanometer particle population became depleted, while the growth within the micrometer range continued. The average particle size provided by the MFI was very large at the start, with a broad range, while the particle counts were very low. These results

are comparable to those obtained when only IgG or dextran sulfate solution was measured, pointing to the presence of small amounts of particulate impurities or contaminants in the starting materials. The average particle size by the end of the experiment was well below 5 µm, which is too small to provide us with reliable morphological parameters[27]. The perikinetic coagulation theory, developed by Smoluchowski about a century ago, predicts the kinetics of particle growth due to Brownian motion driven collision of particles, with subsequent fusion into larger particles[35,36]. This theory has been frequently used to derive information about the time evolution of the particle concentration as they cluster together. For instance, Fisher et al. used a Smoluchowski based population-balance model to describe the precipitation behavior of lysozyme by polyacrylic acid[41]. Chen et al. used Smoluchowski's perikinetic coagulation theory to describe the effect of mixing conditions on the flocculation kinetics of proteins in wastewater[42]. In our study the experimental data was fitted with a simple exponential decay model (Eq. 1), in order to deduce the initial particle concentration (N_0) and the experimental half-life (τ_{exp}). This was performed for 3 different concentrations of the starting materials (with equal mass ratios of the components in each). The physicochemical nature of the formed complexes restricts the success of each collision to fuse into a new larger particle. In case of protein-polyelectrolyte particles the surface could possess a net charge[43], which causes repulsion of similarly charged particles. However, polyelectrolyte bridging in-between particles is the main mechanism behind coagulation of protein-polyelectrolyte complexes[44]. With respect to this restriction, the Smoluchowski model has some limitations, such as the assumptions that the colliding particles are spherical; every collision involves two particles of identical initial size; and each collision leads to a successful fusion[24], meaning that the sticking probability is unity and independent of the particle size. This is very unlikely and probably explains the difference between the experimental and theoretical half-life. With the deduced parameters from the fitting, we have calculated the collision efficiencies, which matched very well between the samples with different IgG and dextran sulfate concentrations.

Conclusion

The combination of NTA and MFI allowed us to analyze the growth kinetics of IgG/dextran sulfate complexes. Our data suggest that electrostatic interactions between IgG and dextran sulfate rapidly lead to the formation of particles. Due to particle collision these primary particles fuse and start to increase in size, leading to a rapid decrease in total nanoparticle concentration and a concomitant increase of new particles that grow further till they reach a size of 1-2 µm. The particle formation process could be described with the coagulation theory of Smoluchowski, provided that a collision efficiency term was introduced. Our approach provides novel insight into the kinetics and mechanism of protein-polyelectrolyte

complex formation and can be applied to other systems, such as complexes between polyelectrolytes and proteins, DNA, or other biomacromolecules.

References

1. Eichler HG, Aronsson B, Abadie E, Salmonson T 2010. New drug approval success rate in Europe in 2009. Nature reviews Drug discovery 9(5):355-356.

2. Leader B, Baca QJ, Golan DE 2008. Protein therapeutics: a summary and pharmacological classification. Nature reviews Drug discovery 7(1):21-39.

3. Mahler HC, Fischer S, Randolph TW, Carpenter JF. 2010. Protein aggregation and particle formation: effects of formulation, interfaces, and drug product manufacturing operations. In Wang W, Roberts CJ, editors. Aggregation of therapeutic proteins, ed., New Jersey: John Wiley & Sons. p 30.

4. Torosantucci R, Schoneich C, Jiskoot W 2014. Oxidation of therapeutic proteins and peptides: structural and biological consequences. Pharmaceutical research 31(3):541-553.

5. Wang W, Nema S, Teagarden D 2010. Protein aggregation--pathways and influencing factors. International journal of pharmaceutics 390(2):89-99.

6. Boeris V, Balce I, Vennapusa RR, Arevalo Rodriguez M, Pico G, Lahore MF 2012. Production, recovery and purification of a recombinant beta-galactosidase by expanded bed anion exchange adsorption. J Chromatogr B Analyt Technol Biomed Life Sci 900:32-37.

7. Xu Y, Mazzawi M, Chen K, Sun L, Dubin PL 2011. Protein purification by polyelectrolyte coacervation: influence of protein charge anisotropy on selectivity. Biomacromolecules 12(5):1512-1522.

8. Chang AC, Gupta RK 1996. Stabilization of tetanus toxoid in poly(DL-lactic-co-glycolic acid) microspheres for the controlled release of antigen. Journal of pharmaceutical sciences 85(2): 129-132.

9. Amidi M, Mastrobattista E, Jiskoot W, Hennink WE 2010. Chitosan-based delivery systems for protein therapeutics and antigens. Adv Drug Deliv Rev 62(1):59-82.

10. Nagpal K, Singh SK, Mishra DN 2010. Chitosan nanoparticles: a promising system in novel drug delivery. Chem Pharm Bull (Tokyo) 58(11):1423-1430.

11. Basak Kayitmazer A, Seeman D, Minsky BB, Dubin PL, Xu Y 2013. Protein-polyelectrolyte interaction. Soft Matter 9:30.

12. Crouzier T, Szarpak A, Boudou T, Auzely-Velty R, Picart C 2010. Polysaccharide-blend multilayers containing hyaluronan and heparin as a delivery system for rhBMP-2. Small 6(5): 651-662.

13. Gormally MV, McKibben RK, Johal MS, Selassie CR 2009. Controlling tyrosinase activity on charged polyelectrolyte surfaces: a QCM-D analysis. Langmuir : the ACS journal of surfaces and colloids 25(17):10014-10019.

14. Lu Y, Wittemann A, Ballauff M 2009. Supramolecular Structures Generated by Spherical Polyelectrolyte Brushes and their Application in Catalysis. Macromol Rapid Comm 30(9-10): 806-815.
15. De Temmerman ML, Rejman J, Vandenbroucke RE, De Koker S, Libert C, Grooten J, Demeester J, Gander B, De Smedt SC 2012. Polyelectrolyte LbL microcapsules versus PLGA microparticles for immunization with a protein antigen. J Control Release 158(2):233-239.
16. Saurer EM, Flessner RM, Sullivan SP, Prausnitz MR, Lynn DM 2010. Layer-by-Layer Assembly of DNA- and Protein-Containing Films on Microneedles for Drug Delivery to the Skin. Biomacromolecules 11(11):3136-3143.
17. McDonald P, Victa C, Carter-Franklin JN, Fahrner R 2009. Selective Antibody Precipitation Using Polyelectrolytes: A Novel Approach to the Purification of Monoclonal Antibodies. Biotechnol Bioeng 102(4):1141-1151.
18. Holler C, Zhang CM 2008. Purification of an acidic recombinant protein from transgenic tobacco. Biotechnol Bioeng 99(4):902-909.
19. Golubovic M, van Hateren SH, Ottens M, Witkamp GJ, van der Wielen LAM 2007. A method for lipase co-precipitation in a biodegradable protein matrix. Biotechnol Bioeng 98(6):1209-1218.
20. Becker AL, Henzler K, Welsch N, Ballauff M, Borisov O 2012. Proteins and polyelectrolytes: A charged relationship. Curr Opin Colloid In 17(2):90-96.
21. Cooper CL, Dubin PL, Kayitmazer AB, Turksen S 2005. Polyelectrolyte-protein complexes. Curr Opin Colloid In 10(1-2):52-78.
22. Kizilay E, Kayitmazer AB, Dubin PL 2011. Complexation and coacervation of polyelectrolytes with oppositely charged colloids. Adv Colloid Interfac 167(1-2):24-37.
23. Clark KM, Glatz CE 1987. Polymer dosage considerations in polyelectrolyte precipitation of protein. Biotechnol Progr 3:6.
24. Meyer CJ, Deglon DA 2011. Particle collision modeling - A review. Miner Eng 24(8):719-730.
25. Carpenter JF, Chemey B, Rosenberg AS. 2012. The critical need for robust assay for quantitation and characterization of aggregates of therapeutic proteins. In Mahler HC, Jiskoot W, editors. Analysis of aggregates and particles in protein pharmaceuticals, ed., New Jersey: John Wiley & Sons.
26. Zolls S, Tantipolphan R, Wiggenhorn M, Winter G, Jiskoot W, Friess W, Hawe A 2012. Particles in therapeutic protein formulations, Part 1: Overview of analytical methods. Journal of pharmaceutical sciences 101(3):914-935.
27. Anderson W, Kozak D, Coleman VA, Jamting AK, Trau M 2013. A comparative study of submicron particle sizing platforms: accuracy, precision and resolution analysis of polydisperse particle size distributions. J Colloid Interface Sci 405:322-330.
28. Carr B, Wright M. 2013. Nanoparticle tracking analysis: A review of applications and usage 2010-2012. ed., Amesbury: NanoSight Ltd.

29. Filipe V, Hawe A, Jiskoot W 2010. Critical evaluation of Nanoparticle Tracking Analysis (NTA) by NanoSight for the measurement of nanoparticles and protein aggregates. Pharmaceutical research 27(5):796-810.
30. Van der Meeren P, Kasinos M, Saveyn H 2012. Relevance of two-dimensional Brownian motion dynamics in applying nanoparticle tracking analysis. Methods in molecular biology 906:525-534.
31. Pedersen JS, Persson M 2014. Unmasking translucent protein particles by improved micro-flow imaging algorithms. Journal of pharmaceutical sciences 103(1):107-114.
32. Telikepalli SN, Kumru OS, Kalonia C, Esfandiary R, Joshi SB, Middaugh CR, Volkin DB 2014. Structural Characterization of IgG1 mAb Aggregates and Particles Generated Under Various Stress Conditions. Journal of pharmaceutical sciences 103(3):796-809.
33. Weinbuch D, Zolls S, Wiggenhorn M, Friess W, Winter G, Jiskoot W, Hawe A 2013. Micro-flow imaging and resonant mass measurement (Archimedes)--complementary methods to quantitatively differentiate protein particles and silicone oil droplets. Journal of pharmaceutical sciences 102(7):2152-2165.
34. Zolls S, Weinbuch D, Wiggenhorn M, Winter G, Friess W, Jiskoot W, Hawe A 2013. Flow imaging microscopy for protein particle analysis--a comparative evaluation of four different analytical instruments. The AAPS journal 15(4):1200-1211.
35. Smoluchowski M 1916. Drei Vorträge über Diffusion, Brownsche Molekularbewegung und Koagulation von Kolloidteilchen. Physikalisch Zeitschrift 17:28.
36. Smoluchowski M 1917. Versuch einer mathematischen Theorie der Koagulationskinetik kolloider Lösungen. Zeitschrift Fur Physikalische Chemie 92:39.
37. Filipe V, Kukrer B, Hawe A, Jiskoot W 2012. Transient molten globules and metastable aggregates induced by brief exposure of a monoclonal IgG to low pH. Journal of pharmaceutical sciences 101(7):2327-2339.
38. Filipe V, Poole R, Oladunjoye O, Braeckmans K, Jiskoot W 2012. Detection and characterization of subvisible aggregates of monoclonal IgG in serum. Pharmaceutical research 29(8):2202-2212.
39. Parker TG, Dalgleish DG 1997. The use of light-scattering and turbidity measurements to study the kinetics of extensively aggregating proteins: alpha-casein. Biopolymers 16:14.
40. Kim WS, Hirasawa I, Kim WS 2001. Effects of experimental conditions on the echanism of particle aggregation in protein precipitation by polyelectrolytes with a high molecular weight. Chem Eng Sci 56:9.
41. Fisher RR, Glatz CE 1988. Polyelectrolyte precipitation of proteins: II. Models of the particle size distributions. Biotechnol Bioeng 32(6):786-796.
42. Chen LA, Serad GA, Carbonell RG 1998. Effect of mixing conditions on flocculation kinetics of wastewaters containing proteins and other biological compounds using fibrous materials and

polyelectrolytes. Brazilian Journal of Chemical Engineering 15:10.

43. Carlsson F, Malmsten M, Linse P 2003. Protein-polyelectrolyte cluster formation and redissolution: a Monte Carlo study. J Am Chem Soc 125(10):3140-3149.

44. Chen W, Walker S, Berg JC 1992. The Mechanism of Floc Formation in Protein Precipitation by Polyelectrolytes. Chem Eng Sci 47(5):1039-1045.